AIAA JOURNAL
Vol. 44, No. 9, September 2006

Investigation over CFD-Based Models for the Identification of Nonlinear Unsteady Aerodynamics Responses

Paolo Lisandrin,* Giampietro Carpentieri,† and Michel van Tooren‡
Delft University of Technology, 2629 HS Delft, The Netherlands

DOI: 10.2514/1.18726

An investigation is performed to assess the importance of the nonlinear effects on the dynamic behavior of a profile in a transonic flow. The analysis is done by applying a system identification approach to a computational fluid dynamics (CFD) code, considered as a black-box system. The CFD code is based on the Euler equations. Both frequency and time domain approaches are used to evaluate the nonlinear effects on the response of different airfoils. The results show that for weak shocks the aerodynamic operator describing the dynamics of the profile around a steady (transonic) flow condition is linear. For strong shocks results obtained with linear models appear to be conservative.

I. Introduction

AEROELASTIC analysis plays a relevant role in aircraft design. In the transonic range, shock waves appear and methods like the doublet lattice, based on linear aerodynamic theories, are no longer applicable. In this case the use of computational fluid dynamics (CFD) tools, based on nonlinear fluid models, becomes a modeling necessity.

In a preliminary design context, Navier–Stokes formulations for the aerodynamics can be computationally too expensive. If viscous effects such as separation or shock-boundary layer interaction are negligible, Euler models are able to capture the relevant nonlinear properties of the fluid, that is, shock location and/or shock movements. On the other hand, when the viscous effects are important, the Euler solution will result in shocks that are typically stronger and farther aft than the shocks computed by a Navier–Stokes solution.

A nonlinear aeroelastic analysis can be performed using different approaches. A first method could be the coupling of the CFD code with a structural code, in a time-marching sense. In this case the large number of unknowns, represented by the structural and aerodynamic grid displacements, result in prohibitive run times for each simulation. Another more efficient approach is the use of modal techniques, expanding the structural displacements as linear combinations of the eigenmodes of the structure (considered as linear throughout this paper).

If the aerodynamic operator is linear, the modal expansion for the displacements leads to the definition of the generalized aerodynamic force (GAF) matrix. This matrix, which is the transfer function between the generalized forces and the modal displacements, depends on both Mach number and reduced frequency. The use of modal techniques results in computationally efficient models, which are widely used for performing linear flutter analysis. For a nonlinear aerodynamic operator, the linear GAF matrix is no longer valid, unless the flow equations are linearized around the (steady) condition of interest. However, the direct linearization of the equations is not a trivial task. Instead, the GAF matrix can be determined using a CFD code as a black-box system: it takes modal displacements as input and gives back generalized forces as output. Using system identification, a reduced order model (ROM) can be created. This model retains the relevant nonlinear properties of the system to be identified, is computationally efficient, and thus well suited for preliminary design applications.

Over the last years significant effort has been spent on the development of ROMs of the unsteady aerodynamic operator, both in frequency and in time domain. Some examples of frequency domain ROMs are the indicial responses by Balhaus and Goorjian [1], the pulse transfer function analysis by Lee-Rausch and Batina [2], field panel method by Fokin [3], Chen [4], Iemma [5], the Volterra theory by Silva [6], Marzocca [7], Raveh [8] and the proper orthogonal decomposition (POD) by Hall [9], Thomas [10]. Examples of time domain ROMs are those based on the auto-regressive moving average model by Cowan [11], Volterra theory by Silva [12], unit sample responses from Gaitonde [13] and the proper orthogonal decomposition by Lucia [14] and Beran [15].

Volterra theory and proper orthogonal decomposition ROMs have received particular attention, as they are applicable to nonlinear systems, whereas the other ROMs are based on linear system representations. The ROMs are intended to represent the dynamics of the (aerodynamic) system around the nonlinear steady state (transonic) flow condition. Such dynamics can be either linear or nonlinear. Silva [6] showed for a NACA0012 profile case the difference in modeling the dynamics as pure linear or linearized from a nonlinear flow condition.

Nevertheless the boundary between modeling the dynamics using a linear or a nonlinear model is not clear. None of the papers mentioned above quantifies the weight of the nonlinear terms in the flow equations or defines clearly the motivation to adopt a linear(-ized) model. They just assume that the nonlinear terms have small contributions by considering small amplitudes of the modal shapes in the system identification procedure. Only Dowell [16] writes that if the nonlinear steady flowfield, including the static shock strength and location, is accurately captured, the dynamic perturbations about the steady flow can be studied using linear models. In any case the results show good agreement with experimental data, in most cases represented by the flutter plot of the well-known AGARD 445.6 wing [17]. The objective of this paper is to investigate whether a ROM suitable for aeroelastic analysis in a preliminary design environment can be derived using a linear system identification procedure. Evidence has been shown for a particular case [18], that even using an Euler code, the aerodynamic system can behave linearly, independent of the amplitude of the input used in the system identification cycle, thus avoiding the use of a nonlinear system identification procedure.

In terms of computational costs the possibility of avoiding a nonlinear system identification procedure is appealing. For example,

Received 11 July 2005; revision received 23 March 2006; accepted for publication 24 March 2006.

*Ph.D. Student, Faculty of Aerospace Engineering; P.Lisandrin@tudelft.nl. AIAA member.

†Ph.D. Student, Faculty of Aerospace Engineering; G.Carpentieri@tudelft.nl. AIAA member.

‡Full Professor, Faculty of Aerospace Engineering; M.J.L.vanTooren@tudelft.nl. MDO TC member.

a Volterra ROM requires that each mode considered is excited separately. Instead, for a linear ROM a multi-input/multi-output (MIMO) identification procedure, requiring only one flow solution, can be used [11]. Besides, in a Volterra based ROM, more than one CFD run is requested for each mode considered. The number of simulations to be performed is depending on the accuracy of the nonlinear approximation. In the following paragraphs, investigations over the influence of the nonlinear terms on the dynamic behavior of a profile in a transonic flow will be performed. This is done by providing the aerodynamic system with suitable inputs, like impulses, having different amplitudes. The computed responses are normalized to the smallest input amplitude. Comparison of these normalized responses together with their frequency content provides a qualitative and quantitative information about the nonlinear behavior of the system.

II. NACA64A010 Test Case

The first test case is based on the NACA64A010 profile studied in the AGARD Report No. 702, case CT6 [19]. This profile has been largely studied in literature. Its importance stems from the fact that when attached to a plunge-pitch spring system, with the structural parameters of the Isogai case [20,21], it exhibits an inviscid limit cycle oscillations phenomenon. For this phenomenon the aerodynamic nonlinearities play a fundamental role. In the AGARD report, case CT6, the profile is set at an angle of attack $\alpha = -0.21$ deg and Mach number $M_\infty = 0.796$. Experimental results (pressure, lift, and pitch moment coefficients) are reported for both a steady analysis and an oscillatory analysis around the quarter chord of the profile.

These results are used as validation data for a computational numerical model built using the commercial package Fluent 6.1.22 [22], based on a finite volume solver of the Euler equations. A second order upwind, implicit scheme has been chosen. The computational domain is circular with a radius which is 40 times the profile chord length. A structured, 80×50 mesh has been chosen after a convergence study on the mesh size. Figure 1 shows the comparison between the numerical and the experimental pressure coefficient (C_p) for the steady analysis performed at $\alpha = -0.21$ deg and $M_\infty = 0.796$. The Mach number at the shock, Fig. 2, is less than 1.2 and the corresponding entropy jump, Fig. 3, is negligible.

Figures 4 and 5, report the lift (c_l) and pitch moment (c_m) coefficient responses versus angle of attack for a sinusoidal oscillation of the profile around its quarter chord, at a reduced frequency of $k_r = 0.202$ ($k_r = \omega b/U_\infty$), with amplitude of $\Delta\alpha = 1.01$ deg. The numerically determined c_l agrees quite well with the experimental one whereas the c_m shows a certain difference. This difference, detected also by other authors [23], is due to the inability of the Euler solver to correctly capture the dynamics of the shock for this particular combination of (large) amplitude/reduced frequency. Nevertheless, the quality of the phenomenon, that is, shock position and boundaries of the c_m, are correctly captured.

The dynamic analysis presented above does not say anything about the expected nonlinear behavior of the system and the importance of the nonlinear terms of the Euler equation to the response of the system. For improved insight, the frequency content of the output is evaluated calculating the Fourier transform of the time histories for the c_l and c_m perturbations. The plots, Figs. 6 and 7,

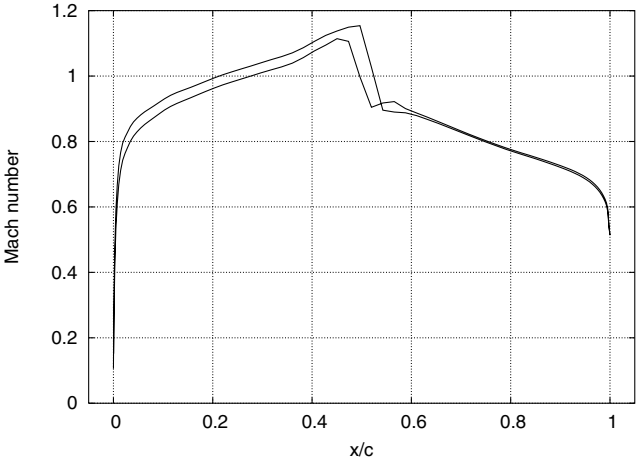

Fig. 2 Mach number along the NACA64A010 profile.

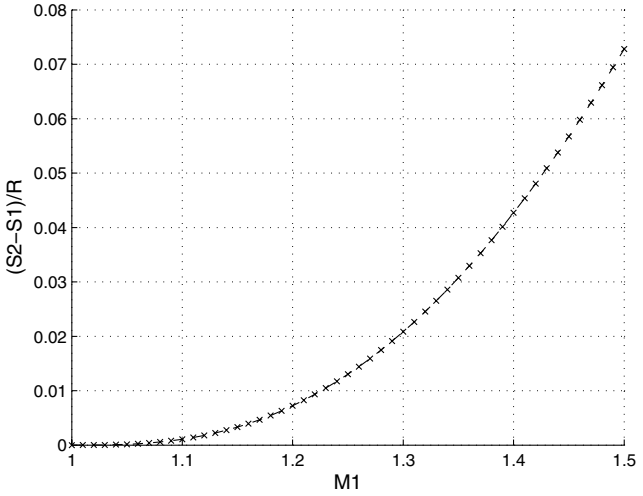

Fig. 3 Variation of the entropy jump with the Mach number ($M1$) before a normal shock.

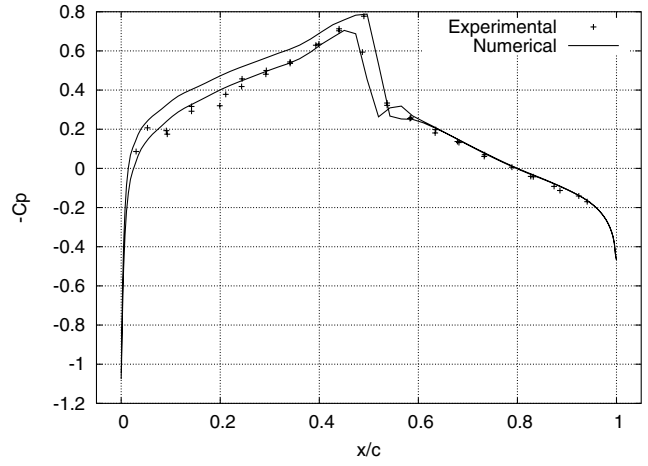

Fig. 1 Pressure coefficient comparison for the steady case, NACA64A010 profile.

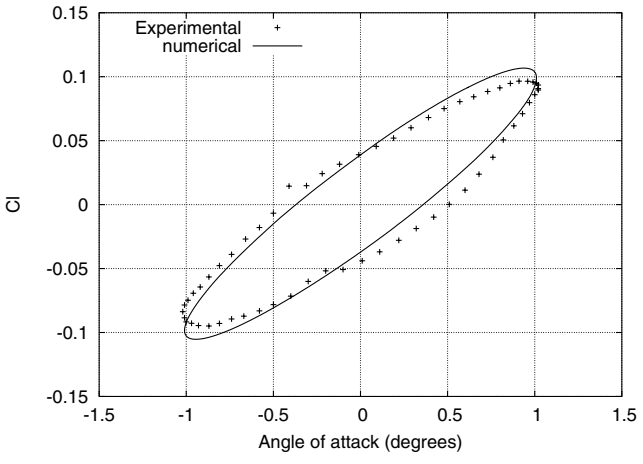

Fig. 4 Lift coefficient versus angle of attack for a sinusoidal oscillation.

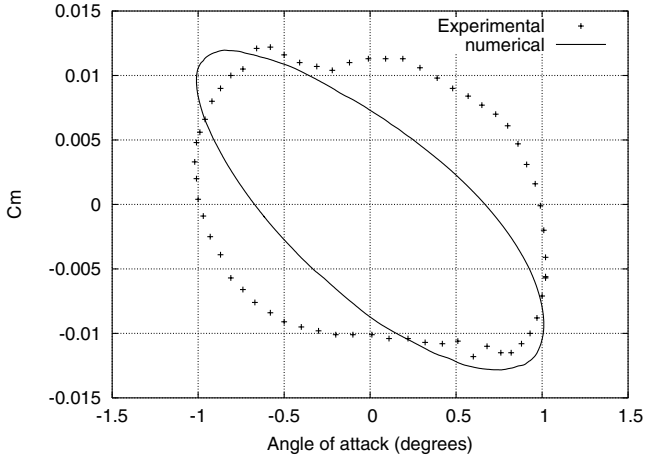

Fig. 5 Moment coefficient versus angle of attack for a sinusoidal oscillation.

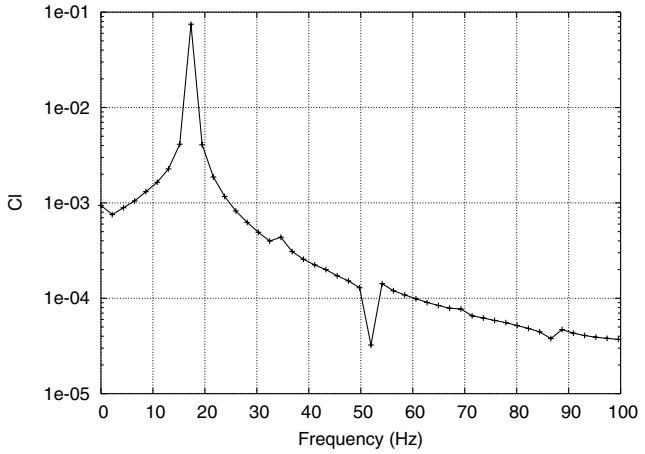

Fig. 6 Modulus of the Fourier transform for the perturbation of the c_l.

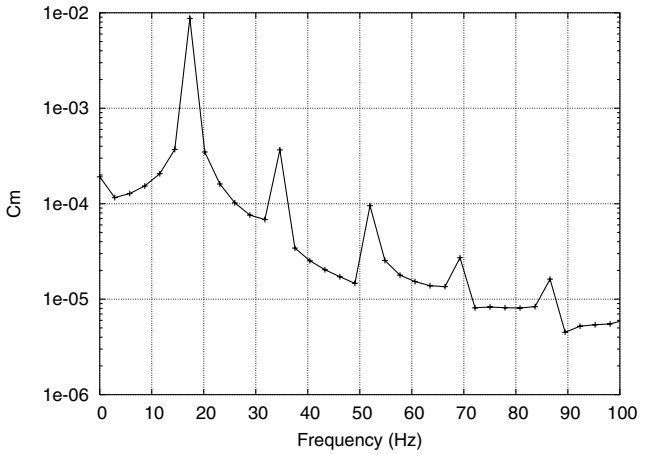

Fig. 7 Modulus of the Fourier transform for the perturbation of the c_m.

show a dominant peak in correspondence of the frequency at which the system has been excited (reduced frequency $k_r = 0.202$ corresponding to a frequency $f = 17.41$ Hz for the undisturbed conditions chosen). More visible on the c_m plot, peaks with decreasing amplitudes appear at frequencies that are a multiple integer of the excitation frequency. The higher frequencies show the contributions of the nonlinear terms in the Euler equations, and they are almost 2 orders of magnitude smaller than the contribution of the input frequency. Of course their influence is expected to grow as the angle of attack around which the analysis is carried on increases, that is, as the shock strength increases.

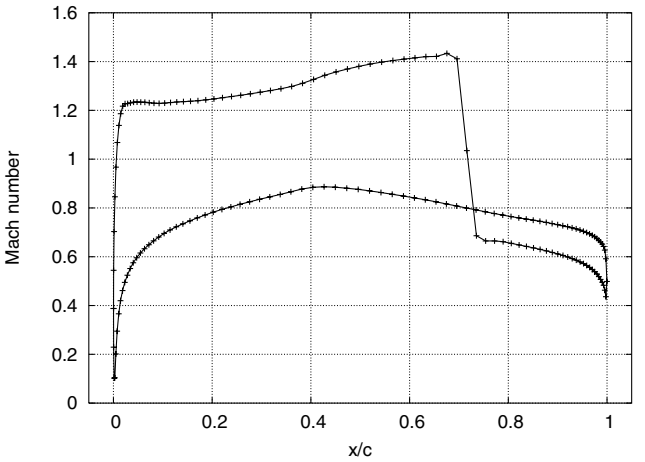

Fig. 8 Mach number over the NACA64A010 profile for a steady angle of attack of 3 deg.

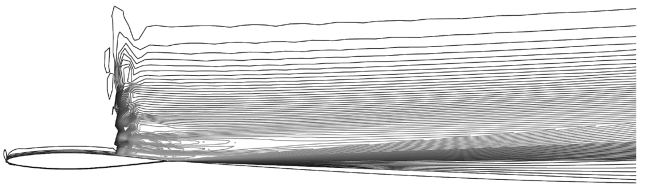

Fig. 9 Entropy contours around the NACA64A010 profile at a steady angle of attack of 3 deg.

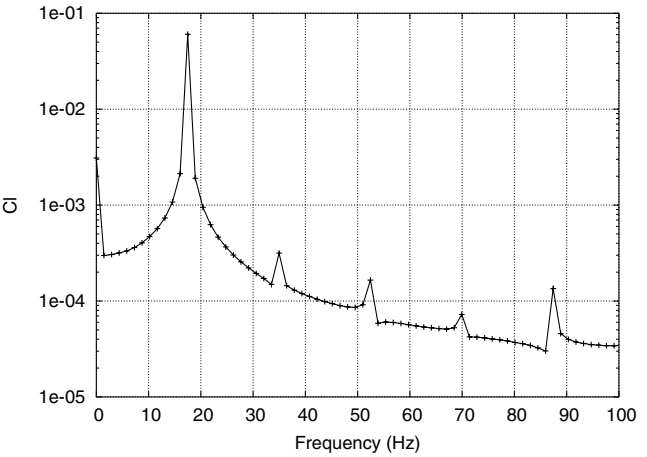

Fig. 10 Modulus of the Fourier transform for the perturbation of the c_l.

To have an idea of the nonlinear effects contribution, a steady analysis has been performed at an increased angle of attack of 3 deg. The shock in this case, Fig. 8, is much stronger. The Mach number before the shock is $M_1 = 1.4$ and the entropy jump is 1 order of magnitude bigger than the previous case at $\alpha = -0.21$ deg. The entropy variation extends through the shock line and it is convected downstream, as shown in Fig. 9. In the previous case the entropy variation is hardly noticeable because it is limited to the root of the shock (for this reason, no contour plot is shown). This case is at the limit of the theoretical capability of the Euler formulation because, in reality, shock-boundary layer interactions can occur and they are not captured by this formulation. Another oscillatory analysis has been done, with an oscillation amplitude of 1 deg around the profile quarter chord. In this case, Figs. 10 and 11, the Fourier transform of the c_l and c_m show obviously an increased contribution of the nonlinear terms. However there is 1 order of magnitude difference between the higher harmonics and the exciting frequency. The results presented thus far show that when the system is excited at one frequency, additional frequencies appear due to the nonlinear

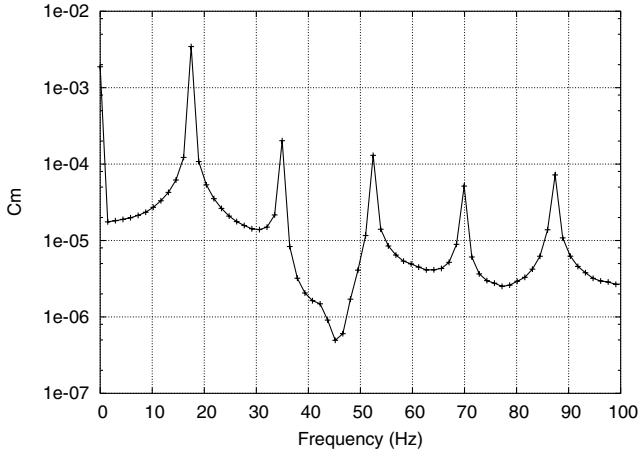

Fig. 11 Modulus of the Fourier transform for the perturbation of the c_m.

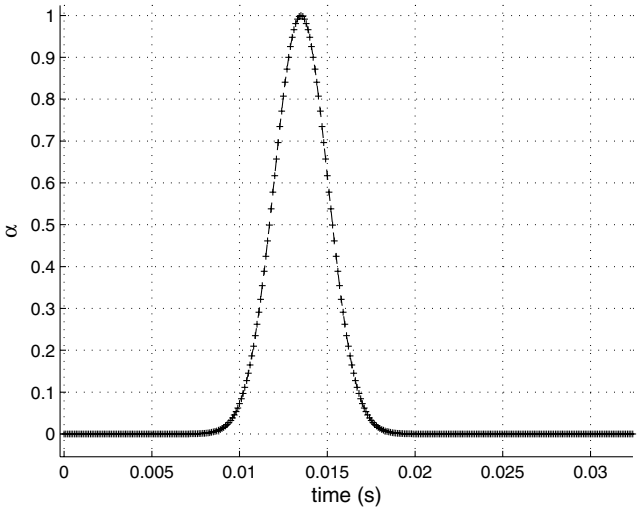

Fig. 12 Time law used for the pitch-angle (α) excitation, normalized to amplitude Amp = 1.

behavior of the system. The contributions of these additional frequencies appear to be negligible and the response of the system can be well represented by the harmonic corresponding to the input frequency.

However, the same conclusion cannot be drawn when the system is excited with a large bandwidth signal, like an impulse. In this case it is not known if the higher harmonics generated by each frequency of the input signal can couple and still have a negligible effect on the system response.

To investigate the occurrence of this effect, the same oscillatory analysis is performed using a typical input employed in system identification, consisting of a Gaussian shaped impulse called "enlarged impulse," Fig. 12. In the present case the time law for the perturbation in the angle of attack α is defined by

$$\alpha(t) = \mathrm{Amp} \cdot e^{-\left[\frac{t-\frac{T_{\mathrm{imp}}}{2}}{K \cdot T_{\mathrm{imp}}}\right]^2} \tag{1}$$

where T_{imp} is the time interval during which the function is not zero, Amp is the amplitude of the input function, K a factor that determines the smoothness of the derivatives of the input signal at the time zero and T_{imp} [24]. In the present work the parameters have been chosen such that the bandwidth equals a reduced frequency of $k_r = 1$, Fig. 13, resulting in $K = 0.08$ and $T_{\mathrm{imp}} = 0.027$ s. A better insight to the procedure used to define all the parameters for the excitation of the system and the relation to the physical parameters of the problem,

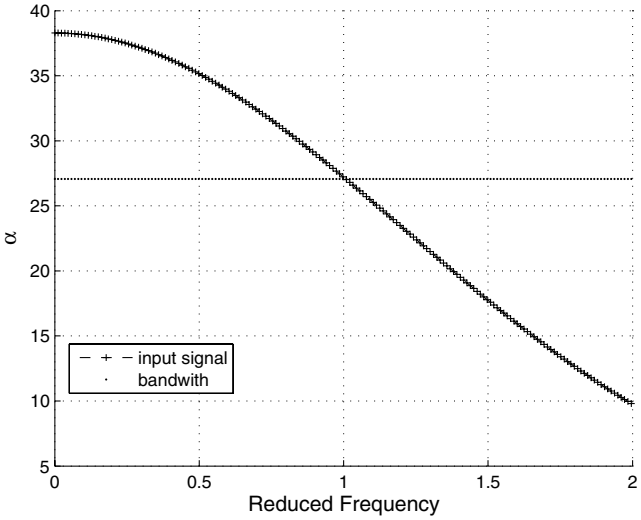

Fig. 13 Modulus of Fourier transform of the pitch-angle (α) excitation.

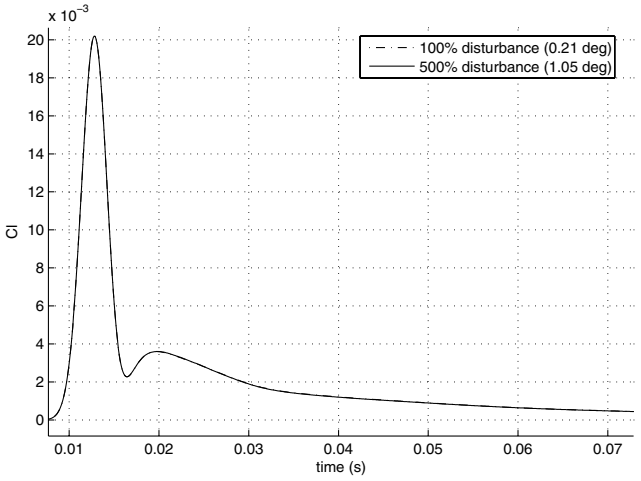

Fig. 14 Scaled time histories of c_l for different perturbations around 0.21 deg steady angle of attack.

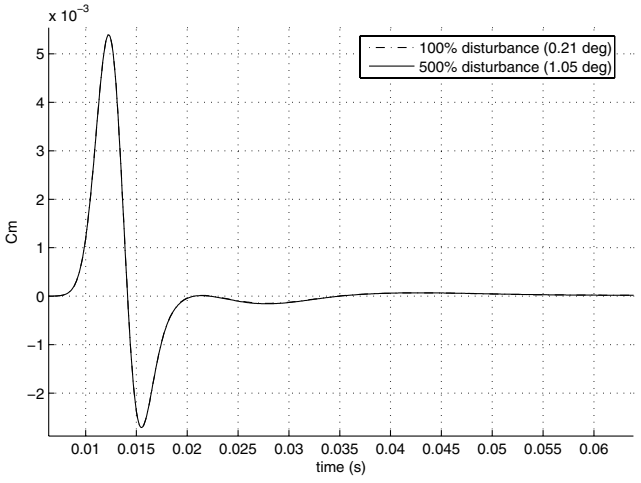

Fig. 15 Scaled time histories of c_m for different perturbations around 0.21 deg steady angle of attack.

such as Mach number and frequency bandwidth, can be found in [25].

Again a pitch motion, with time history defined by the enlarged impulse, has been assigned to the profile set at an angle of attack of $\alpha = -0.21$ deg. Two different pitch amplitudes have been selected

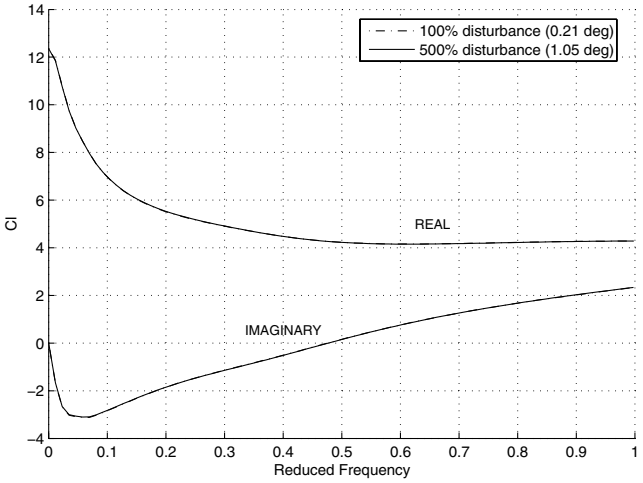

Fig. 16 Real and imaginary parts of the Fourier transforms of the scaled time histories of c_l for different perturbations around 0.21 deg steady angle of attack.

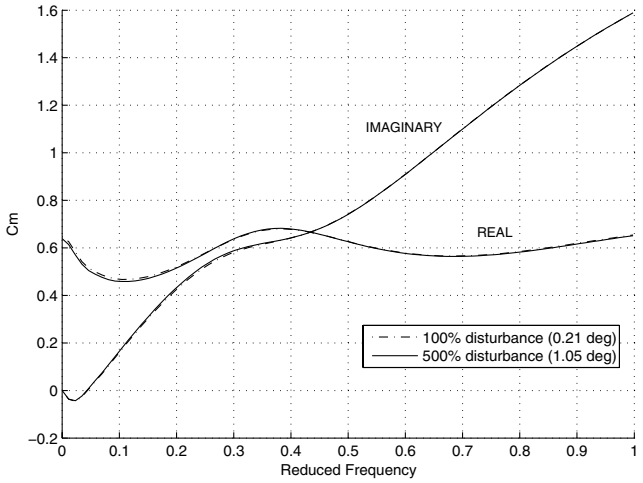

Fig. 17 Real and imaginary parts of the Fourier transforms of the scaled time histories of c_m for different perturbations around 0.21 deg steady angle of attack.

for the analysis, $\text{Amp}_1 = 0.21$ deg and $\text{Amp}_2 = 1.05$ deg. These amplitudes correspond, respectively, to a perturbation of 100% and 500% of the steady angle of attack, and they are both far from the assumption of "small" perturbations. For each simulation, the time histories of the c_l and c_m as well as the shock movement have been recorded. A linearity check of the system's behavior has been performed normalizing the responses to the smallest amplitude of the input signals: in Figs. 14 and 15 the scaled time histories of the c_l and the c_m are reported, limited to a time range where the transient response is appreciable. As can be seen, the two curves lie on top of each other. A better insight of the system's behavior is gained performing a frequency domain analysis. Thus for each time history a Fourier transform has been calculated and divided by the Fourier transform of the corresponding input, frequency by frequency. For a linear system, this procedure provides the transfer function of the system, which is independent of the amplitude of the input signal. In particular, for an aerodynamic linear system, this gives the contribution of the pitch mode to the generalized aerodynamic force matrix. For a nonlinear system, as the present case, this approach can only quantify the magnitude of the nonlinearities, as the scaled responses depend on the input's amplitude.

Figures 16 and 17 show that the scaled responses overlap for each frequency of the bandwidth of interest, thus the system behaves linearly. In this case the shock measured oscillation is far below 1% of the chord length, and its strength is defined by the steady flow condition, Fig. 2, with negligible entropy loss. For this particular

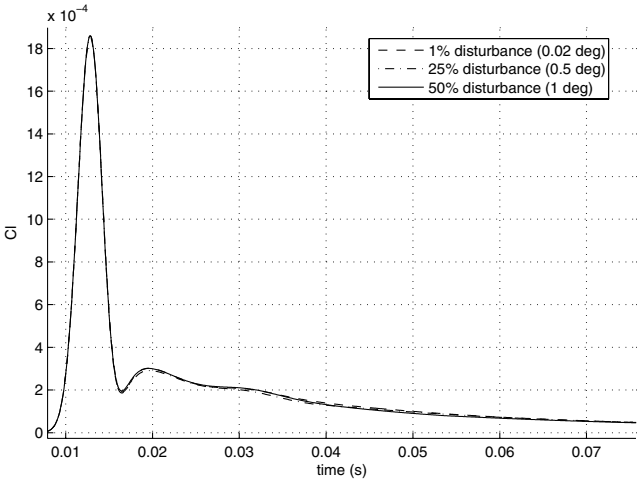

Fig. 18 Scaled time histories of c_l for different perturbations around 2 deg steady angle of attack.

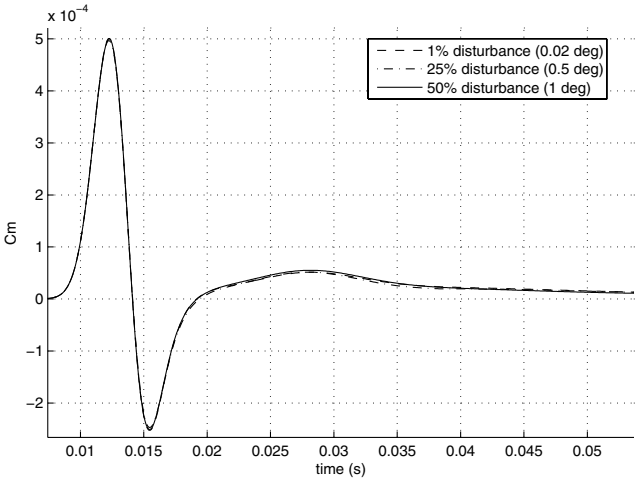

Fig. 19 Scaled time histories of c_m for different perturbations around 2 deg steady angle of attack.

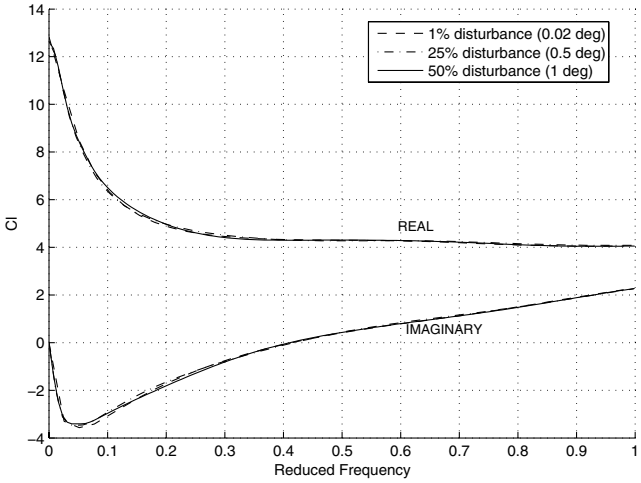

Fig. 20 Real and imaginary parts of the Fourier transforms of the scaled time histories of c_l for different perturbations around 2 deg steady angle of attack.

shock strength/movement combination a linear model for the dynamics of the system is appropriate.

To check the validity range of the system's linearity, it is useful to carry the previous analysis around a condition in which the shock strength is increased. For this purpose the analysis is performed about

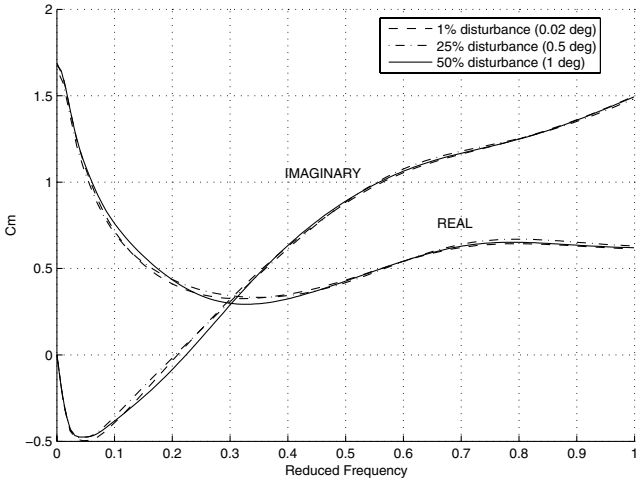

Fig. 21 Real and imaginary parts of the Fourier transforms of the scaled time histories of c_m for different perturbations around 2 deg steady angle of attack.

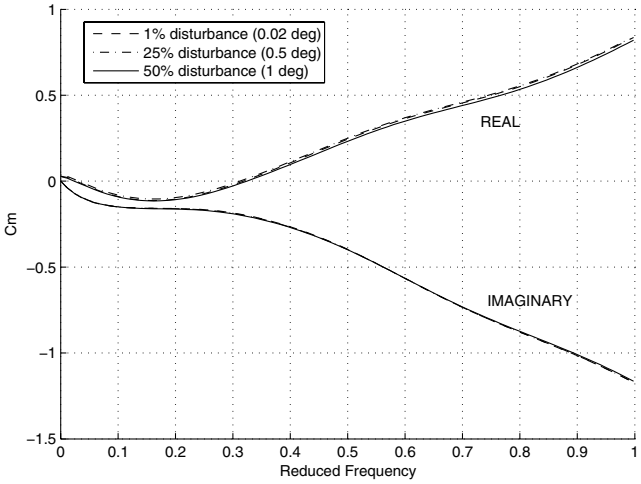

Fig. 23 Real and imaginary parts of the Fourier transforms of the scaled time histories of c_m for different perturbations of the plunge velocity at a 2 deg steady angle of attack.

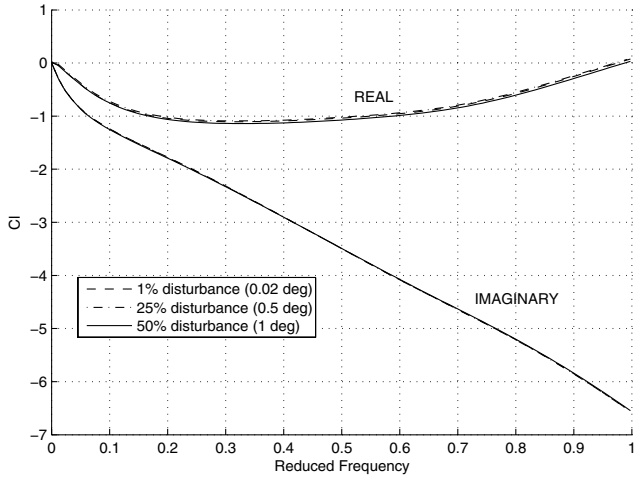

Fig. 22 Real and imaginary parts of the Fourier transforms of the scaled time histories of c_l for different perturbations of the plunge velocity at a 2 deg steady angle of attack.

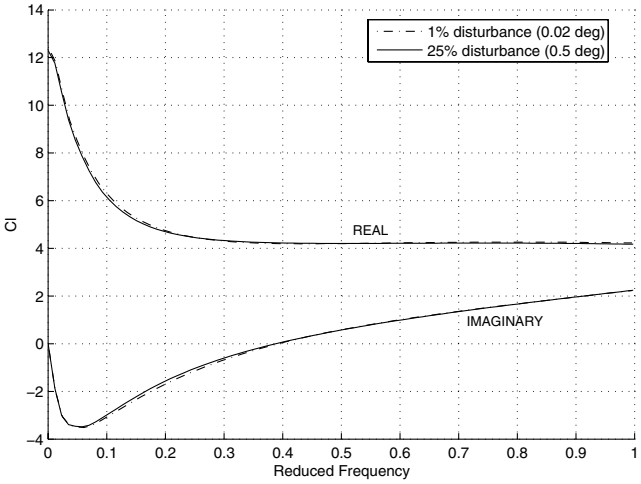

Fig. 24 Real and imaginary parts of the Fourier transforms of the scaled time histories of c_l for different perturbations around 2 deg steady angle of attack, MBBA3 profile.

2 deg angle of attack. In this condition the shock is strong, and again a shock boundary-layer interaction is a physical possibility that the Euler solution cannot capture. Figures 18 and 19 display the scaled time histories of c_l and c_m for 1, 25, and 50% perturbation of the steady angle of attack. The responses show more differences than the 0.21 deg angle of attack case, and still they are not clearly noticeable. Again the differences are more appreciable if the Fourier transform is calculated. Figures 20 and 21 show the real and imaginary parts of the Fourier transform of the c_l and c_m divided by the Fourier transform of their respective input. Differences between the various input amplitudes can be noticed especially for the c_m. In this case the shock movement ranges from values between 0.6% and 1.5% of the chord with a slight change in its strength compared to the steady value. The differences between the curves are such that the dynamics of the (aerodynamic) system can be considered linear. For a linear system the quantities calculated are the contribution of the pitch mode to the generalized aerodynamic force matrix, which consists also of the generalized forces due to the plunge mode of the profile. For a complete understanding, the procedure performed previously for the pitch motion has been applied also for the plunge mode. The plunge motion is assigned in terms of (vertical) velocity. The amplitude of this motion is taken equal to the maximum velocity reached by the profile during the pitch motion (i.e., vertical velocity at the trailing edge). This way, the perturbations of the plunge and pitch modes are comparable. Figures 22 and 23 show again that the system response to the plunge motion is almost independent from the magnitude of the input, with the nonlinear effects even less evident than the pitch motion case.

The analyses and results presented so far have been applied to one profile only. The linear behavior shown in the results cannot be generalized to any profile. To get a more general understanding, the same linearity check has been performed on two other different profiles for the pitch motion case, which is the most important for the appearance of the nonlinear effects.

III. MBBA3 Test Case

The MBBA3 profile is a supercritical profile with a maximum thickness of 8.9%, shockfree for the design conditions of $M_\infty = 0.76$, $\alpha = 1.3$ deg. The analysis has been performed taking a steady condition with the same design Mach number and an off-design steady angle of attack of 2 deg. In this case the Mach number at the shock reaches the maximum value of about $M_1 = 1.4$. A linearity check has been performed assigning two inputs: a small amplitude input, equal to 1% of the steady angle of attack and a "large" amplitude input equal to 25% of the same angle. Figures 24 and 25 show the Fourier transforms for the scaled responses of c_l and c_m. Negligible differences can be noticed between the different responses, therefore the dynamics of the profile can be considered linear. The results agree with those found in [26].

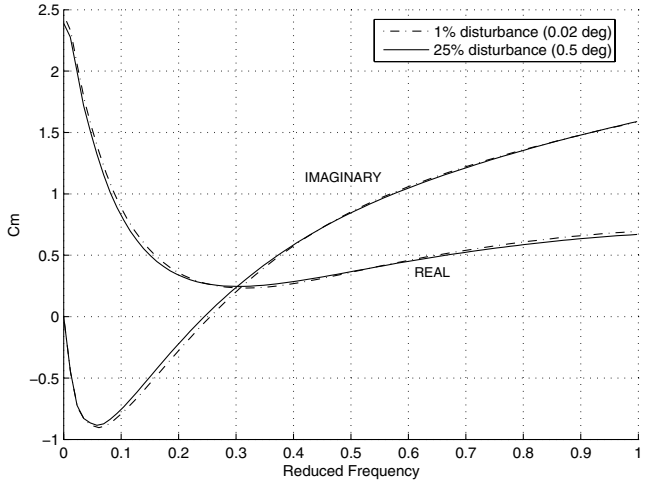

Fig. 25 Real and imaginary parts of the Fourier transforms of the scaled time histories of c_m for different perturbations around 2 deg steady angle of attack, MBBA3 profile.

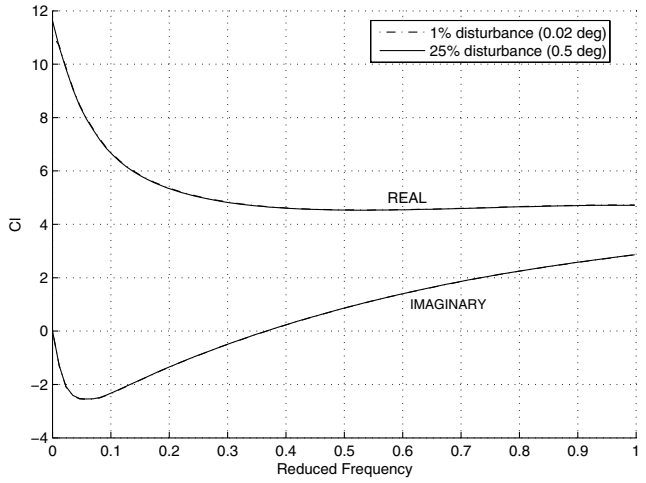

Fig. 26 Real and imaginary parts of the Fourier transforms of the scaled time histories of c_l for different perturbations around 2 deg steady angle of attack, RAE2822 profile.

IV. RAE2822 Test Case

The RAE2822 profile is a subcritical profile with a maximum thickness of 12.1%. Also for this profile a linearity check has been performed around a steady angle of attack of 2 deg, a condition at which a strong shock (Mach number at the shock around 1.4) appears. A pitch motion has been assigned using the same amplitudes of the MBBA3 profile. Figures 26 and 27 show again that the dynamics around the steady condition is linear.

V. Flutter Results

A first flutter analysis with the V–g method has been performed for the NACA64A010 airfoil, at an angle of attack of −0.21 deg, using the components of the GAF matrix shown in Figs. 17 and 18. The contribution of the plunge motion to the GAF matrix has been calculated, but the plots are not reported here. The values for the structural parameters refer to the Isogai case of NACA64A010 [20].

Table 1 reports the flutter speed index $V^* = U_{\text{fl}}/(b\omega_\alpha\sqrt{\mu})$ (U_{fl} is the dimensional flutter velocity, b is the semichord, ω_α is the torsional spring stiffness, and μ is the mass ratio [20,27], defined as $\mu = m/\pi\rho b^2$), the reduced frequency, and the percentage variation in the flutter speed index with respect to the 100% perturbation case. The results show that the variation in the flutter speed index is negligible, in agreement with the results of the linearity check shown in Figs. 17 and 18.

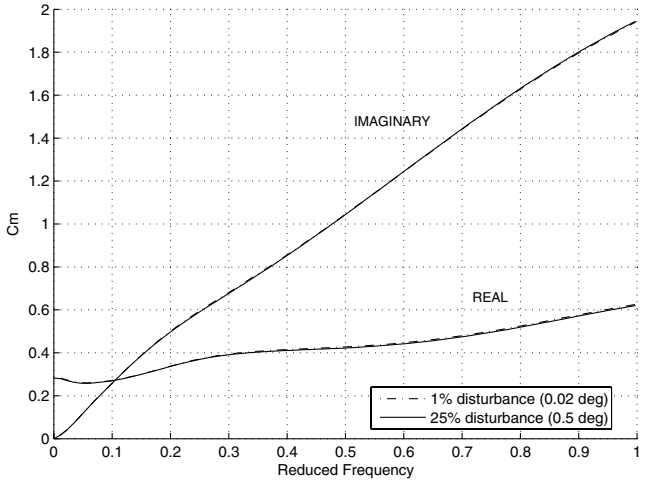

Fig. 27 Real and imaginary parts of the Fourier transforms of the scaled time histories of c_m for different perturbations around 2 deg steady angle of attack, RAE2822 profile.

Table 1 Flutter speed indexes corresponding to different impulse amplitudes used for the GAF matrix construction for the 0.21 deg angle of attack case

Impulse case/amplitude	Flutter speed index V^*	Reduced frequency	Difference with V^* of case 1
1–100%	1.154	0.132	0
2–500%	1.152	0.132	0.17%

Table 2 Flutter speed indexes corresponding to different impulse amplitudes used for the GAF matrix construction of the 2 deg angle of attack case

Impulse case/amplitude	Flutter speed index V^*	Reduced frequency	Difference with V^* of case 1
1–1%	1.410	0.136	0
2–25%	1.430	0.137	1.41%
3–50%	1.468	0.141	4.11%

The flutter analysis has been repeated for the NACA64A010 airfoil, at an angle of attack of 2 deg, using the GAF matrix components shown in Figs. 21–24. Table 2 reports the flutter speed index, the reduced frequency, and the percentage variation in the flutter speed index with respect to the 1% perturbation case. In this case the variations are more evident. However, they are limited to a maximum of 5%, even when the input amplitude is increased by 50% with respect to the reference case, thus proving the outcomes of the linearity checks. The results also show that the flutter speed index variations due to the differences in the components of the GAF matrix are "robust." Besides, the flutter speed index has a "tendency" to conservativism, as increasing the input amplitude increases the flutter velocity.

VI. Conclusions

The flutter results presented for the NACA64A010 airfoil show that for the particular case analyzed the aerodynamic operator can be considered linear with respect to perturbations of the displacements around the steady condition, as long as flow separations or shock-boundary layer interactions do not occur, that is, an Euler model for the flowfield can be assumed. This linear behavior can be attributed to the small excursion of the shock from its steady position, regardless of the small or large displacements given to the airfoil. Indeed the shock motion is limited to less than 2% in the worst case analyzed. In this situation a flutter analysis can therefore be

performed using the traditional modal approach which leads to the definition of the GAF matrix. Where analytical expressions are not available for the GAF matrix a system identification approach can be used, providing a CFD code with suitable inputs and recording the outputs. A linear system identification tool can be used producing results that have been shown to be robust and conservative.

References

[1] Ballhaus, W. F., and Goorjian, P. M., "Computation of Unsteady Transonic Flows by Indicial Methods," *AIAA Journal*, Vol. 16, No. 2, 1978, pp. 117–124.

[2] Lee-Rausch, E. M., and Batina, J. T., "Wing Flutter Boundary Prediction Using Unsteady Euler Aerodynamic Method," *Journal of Aircraft*, Vol. 32, No. 2, 1995, pp. 416–422.

[3] Fokin, D., Gebhardt, L., Lutz, T., and Wagner, S., "A Field-Panel Approach for Flow Calculation about 3D Transonic Configurations," *Proceedings of the Twenty-Third International Conference on the Boundary Element Method*, WIT Press, Billerica, MA, 2001, pp. 207–216.

[4] Chen, P. C., Gao, X. W., and Tang, L., "Overset Field-Panel Method for Unsteady Transonic Aerodynamic Influence Coefficient Matrix Generation," *AIAA Journal*, Vol. 42, No. 9, Sept. 2004, pp. 1775–1786.

[5] Iemma, U., Gennaretti, M., "Reduced-Order Modeling for Linearized Aeroelasticity of Fixed Wings in Transonic Flight," *Journal of Fluids and Structures*, Vol. 21, No. 3, 2005, pp. 243–255.

[6] Silva, W. A., "Discrete-Time Linear and Nonlinear Aerodynamic Impulse Responses for Efficient CFD Analysis," Ph.D. Dissertation, Faculty of the Department of Applied Sciences, College of William and Mary, Williamsburg, VA, Oct. 1997.

[7] Marzocca, P., Librescu, L., and Silva, W. A., "Volterra Series Approach For Nonlinear Aeroelastic Response of 2-D Lifting Surfaces," AIAA Paper 2001-1459, 2001.

[8] Raveh, D., Levy, Y., and Karpel, M., "Efficient Aeroelastic Analysis Using Computational Unsteady Aerodynamics," *Journal of Aircraft*, Vol. 38, No. 3, 2001, pp. 547–556.

[9] Hall, K. C., Thomas, J. P., and Dowell, E. H., "Proper Orthogonal Decomposition Technique for Transonic Unsteady Aerodynamic Flows," *AIAA Journal*, Vol. 38, No. 10, 2000, pp. 1853–1862.

[10] Thomas, J. P., Dowell, E. H., and Hall, K. C., "Three-Dimensional Transonic Aeroelasticity Using Proper Orthogonal Decomposition Based Reduced Order Models," *Journal of Aircraft*, Vol. 40, No. 3, May–June 2003, pp. 544–551.

[11] Cowan, T. J., Arena, A. S., Jr., and Gupta, K. K., "Accelerating Computational Fluid Dynamics Based Aeroelastic Predictions Using System Identification," *Journal of Aircraft*, Vol. 38, No. 1, 2001, pp. 81–87.

[12] Silva, W. A., and Bartels, R. E., "Development of Reduced-Order Models for Aeroelastic Analysis and Flutter Prediction Using the CFL3Dv6.0 Code," *Journal of Fluids and Structures*, Vol. 19, No. 6, 2004, pp. 729–745.

[13] Gaitonde, A., and Jones, D. P., "Reduced Order State-Space Models from the Pulse Responses of a Linearized CFD Scheme," *International Journal for Numerical Methods in Fluids*, Vol. 42, No. 6, 2003, pp. 581–606.

[14] Lucia, D. J., Beran, P. S., and King, P. I., "Reduced Order Modelling for an Elastic Panel in Transonic Flow," AIAA 2002-1594, 2002.

[15] Beran, P. S., Lucia, D. J., and Pettit, C. L., "Reduced Order Modeling of Limit Cycle Oscillation for Aeroelastic Systems," *Journal of Fluids and Structures*, Vol. 19, No. 5, 2004, pp. 575–590.

[16] Dowell, E. H. (ed.), *A Modern Course in Aeroelasticity*, 3rd revised and enlarged edition, Kluwer, Dordrecht, The Netherlands, 1995.

[17] Yates, E. C., Jr., "AGARD Standard Aeroelastic Configurations for Dynamic Response. Candidate Configuration I.—Wing 445.6," NASA TM-100492, 1987.

[18] Liani, E., "Identification of Aeroelastic Systems in Transonic Flows," M.S. Thesis, Università degli Studi di Roma "La Sapienza," Roma, Italy, July 2004.

[19] Davis, S. S., "NACA 64A010 (NASA Ames Model) Oscillatory Pitching," AGARD Rept. 702, Jan. 1982.

[20] Isogai, K., "On the Transonic-Dip Mechanism of Flutter of a Sweptback Wing," *AIAA Journal*, Vol. 17, No. 7, 1979, pp. 793–795.

[21] Isogai, K., "Transonic Dip Mechanism of Flutter of a Sweptback Wing. II," *AIAA Journal*, Vol. 19, No. 9, 1981, pp 1240–1242.

[22] AA.VV, *Fluent 6.0 User's Guide*, Fluent.Inc., Nov. 2001.

[23] McMullen, M., Jameson, A., and Alonso, J., "Application of a Non-Linear Frequency Domain Solver to the Euler and Navier-Stokes Equations," AIAA 2002-120, 2002.

[24] Lazzaro, R., Mastroddi, F., and Lisandrin, P., "Identification of Linear and Non-Linear Aeroelastic Systems Through Volterra Series Approach," *Proceedings of the XVII AIDAA Conference*, Vol. 2, pp. 983–996, AIDAA Associazione Italiana di Aeronautica e Astronautica Editor, Rome, Italy, 2003.

[25] Lisandrin, P., van Tooren, M. J. L., "Identification of the Aerodynamic Properties of Non-Linear Wing Systems," *39th Erice Workshop: Design Challenges and Mathematical Methods in Aircraft and Spacecraft*, 2003 (to be published).

[26] Bland, R. S., and Edwards, J. W., "Airfoil Shape and Thickness Effects on Transonic Airloads and Flutter," NASA TM 84632, March 1983.

[27] Prananta, B. B., Kok, J. C., Spekreijse, S. P., Hounjet, M. H. L., and Meijer, J. J., "Simulation of Limit Cycle Oscillations of Fighter Aircraft at Moderate Angle of Attack," NLR TP-2003-526, Oct. 2003, http://www.nlr.nl/documents/publications/2003/2003-526-tp.pdf.

K. Ghia
Associate Editor